© Indian Academy of Sciences

Magnetic fabrics and magnetic mineralogical variations in Lava Channel: An example from the Deccan Volcanic Province, India

S J Sangode[1,*], Sayelli Tembhurne[1,2], Rasika Mahajan[1,3], K Deenadayalan[4], D C Meshram[1], A N Dongre[1], Amarjeet R Bhagat[1] and K V V Satyanarayana[4]

[1]*Department of Geology, Savitribai Phule Pune University, Pune 411 007, India.*
[2]*Present address: Central Ground Water Board, Jaipur, India.*
[3]*Present address: Scottish Universities Environmental Research Centre, Glasgow, UK.*
[4]*Indian Institute of Geomagnetism, New Panvel, Navi Mumbai 410 218, India.*
*Corresponding author. e-mail: sangode63@gmail.com

A $\sim$3000 m long exposure of paleo-lava channel body within the Deccan volcanic province (India) has been investigated for mineral magnetism and anisotropy of magnetic susceptibility (AMS) to examine the lava flow-related fabrics. Distinct gradient from ferrimagnetic to antiferromagnetic mineralogy along the channel indicated progressive oxidative mixing. The AMS studies along and across the channel profiles decipher a combination of factors responsible for the resultant fabrics. Various dominating mechanisms including gravity settling, grain imbrications, viscous shear and competitive mineral readjustments penultimate to cooling appears to have imparted the final/resultant fabric. The orientation of principle susceptibility axes (K1-K2-K3) and petrographic observations define three major types of fabrics as: (I) mineral lineation, (II) crystal settling and (III) crystal-matrix-re-adjustment. The resultant of type I along with imbrications is generally observed along the axial part, while type II are developed during lava residency; and the opaque−non-opaque interlocking with groundmass resulted in type III fabrics. A three-stage model is produced to resolve the plausible sequence of fabric development during various stages of the lava flow formation. More detailed AMS studies on the Deccan lavas are envisaged to lead semi-quantitative information on fluid dynamical forces governed by slope gradients and gravity, dynamic thermal changes in viscosity, shear and the effects of paleotopography.

Keywords. Deccan traps; rock magnetism; anisotropy of magnetic susceptibility; lava channel; petrofabrics.

1. Introduction

Deccan volcanic province (DVP) in India represents >2000 m thick lava pile, covering an area >500,000 km^2 and is one of the largest igneous provinces of the world (Mahoney 1988; Subbarao 1988; Hooper 1990). Studies on the Deccan traps present detailed work on petrogenesis and geochemical and/or isotopic signatures, architectural and emplacement dynamics, stratigraphy,

paleomagnetism and magnetostratigraphy, paleointensity, age and climatic−biotic impacts (e.g., Cox and Hawkesworth 1985; Vandamme *et al.* 1991; Bondre *et al.* 2004; Chenet *et al.* 2008, 2009; Duraiswami *et al.* 2014; Font *et al.* 2018; Radhakrishna *et al.* 2020; Dongre *et al.* 2021). However, little quantitative information is available on the microscopic fabrics that can have great implications in understanding more advanced aspects such as flow dynamics and viscosity shear within individual lava flows (e.g., Sangode *et al.* 2017). The Deccan trap basalts essentially represent ferrimagnetic fabrics within a silicate matrix of paramagnetic minerals (e.g., olivine, pyroxene and feldspars). The resultant fabrics although are dominated by ferromagnesian minerals, their orientation might have been greatly influenced by multiple mechanisms of flow dynamics and cooling history. Detailed studies on petrofabrics may address several issues such as rheology of the lava flow, gravity settling of minerals, dynamic viscosity at variable cooling temperatures, viscosity shear, interaction with matrix and the ductile deformation amongst the Deccan lava flows. The ultimate fabrics can be resolved using petrofabric methods like anisotropy of magnetic susceptibility (AMS), which represent an advanced instrumental technique supported by several case studies (e.g., Rochette *et al.* 1991, 1992; Cañón-Tapia 1994; Zhang and Piper 1994; Tauxe *et al.* 1998; Cañón-Tapia and Pinkerton 2000; Callot *et al.* 2001; Herrero-Bervera *et al.* 2001; Geoffroy *et al.* 2002; Mamtani and Greiling 2005; Zak *et al.* 2008; Majumder and Mamtani 2009).

In basalts, the AMS can result from the shape and distribution (internal arrangement) of ferrimagnetic grains and/or the magnetocrystalline anisotropy. These parameters are further affected by: (i) domain size and geometry of the grains (Rochette *et al.* 1991, 1992), (ii) magnetic interactions due to distribution of ferrimagnetic particles (Hargraves *et al.* 1991; Stephenson 1994), (iii) strain variations experienced by the grains after viscous flow (Dragoni *et al.* 1997) and (iv) postemplacement stresses and alterations (Ellwood 1981; Park *et al.* 1988; DeWall *et al.* 2010). Fluid dynamical and gravitational forces tend to control the resultant anisotropy providing ultimate petrofabric in the rocks after cooling. Additionally, the complex processes such as viscosity shear, penecontemporaneous or post-emplacement stresses and deformations do have a large scope to alter the early fabrics (e.g., Cañón-Tapia 1996). Hence, a combination of processes needs to be evaluated before the interpretation of AMS data, especially when the fabrics are random and un-clustered at sample level or site level as discovered in many flows in Deccan traps elsewhere (e.g., Sangode *et al.* 2017). Therefore, studies are needed from well-defined morphological features such as channel or tunnel.

The application of AMS is implemented as a rapid yet sensitive tool to determine resultant fabrics in basaltic magma flows (e.g., Cañón-Tapia and Pinkerton 2000; Cañón-Tapia and Coe 2002; Bascou *et al.* 2005). Once established, these studies can provide quantitative database to understand the fluid-dynamical mechanism of the lava flows. Moreover, the parameters established from outcrop studies can be evolved for better interpretation of AMS data from borehole cores. AMS is based on the first-order rock magnetic parameter of magnetic susceptibility, it is, therefore, essential to know the state of magnetic minerals (type, concentration, domain size and their mixtures) to understand the mineralogic controls of AMS. In Deccan traps, these studies are essential to characterise the lava flow units and its lateral correlations to establish high-resolution stratigraphy. In this initial stage, it, therefore, needs several experimental attempts to develop precise inferences from AMS. Well-documented morphological features such as lava flow channels and tunnels are therefore best laboratory to develop the AMS study. A previously reported lava flow channel (Sen *et al.* 2012) near Nashik in western Maharashtra hence was selected for the present attempt.

2. Study area and methods

We sampled the lava channel exposed at Vadali Bhoi (20°16′50″N, 74°06′20″E), near Khedrai dam (in the vicinity of Khedrai Mata temple) in the north-eastern part of Nashik (or Nasik) district of Western Maharashtra (figure 1).

This lava channel first reported by Mishra *et al.* (2001) is exposed as low height mounds, east and southeast of Vadali Bhoi (figures 1 and 2). A spillway (*Nala*) east of the dam, exposes good cross sections of the channel measuring the widths from about <100 to ∼125 m. The channel-fills are exposed in contact with the substrate representing Giant Plagioclase Basalt (GPB). The channel shows pairs of levees (figure 2) and there is absence of any roof-like crust throughout the erosional
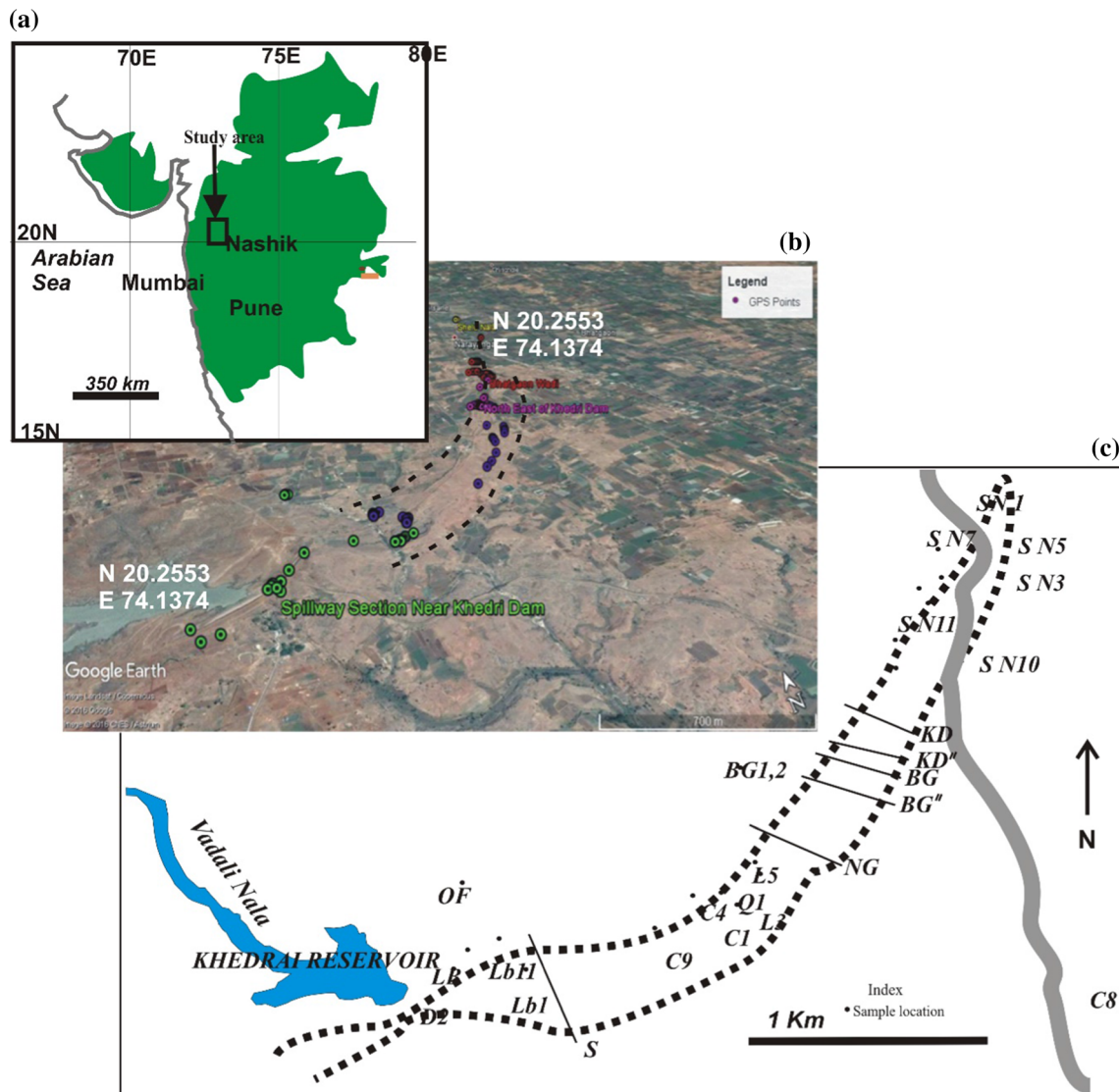
Figure 1. (**a**) Schematic map of the Deccan traps province re-drawn after Hooper (1990); (**b**) geologically mapped outline of the Khedrai lava channel (mapped from Google Earth image, fieldwork and from Sen *et al.* 2012) depicting its curvilinear nature and extent.

outcrop to suggest a tunnel morphology. The remnants of the channel are aligned in curvilinear manner (figure 2) with a dominant NE–SW trend towards the north continuing up to the villages, Bhatgaonwadi and Narayangao (figure 1).

The dominant lithology in the Khedrai channel is GPB and is similar to the GPB occurrences in Igatpuri, Neral, Bhimashankar and Khandala formations in the Western Deccan provinces. The plagioclase megacrysts are present both within the substrate pahoehoe flow and the channel, suggesting it as the topmost flow of the Lower Ratangarh Formation equivalent to M2-GSI-1989 (Godbole *et al.* 1996; Sen *et al.* 2012). This formation is also equivalent to Igatpuri Formation, which is characterised by high phenocryst ratio of more than 0.7 (Beane and Hooper 1986; Nair and Bhusari 2001;

Sen *et al.* 2012). The GPB in field shows randomly oriented laths of plagioclase ranging from ~ 30 mm in length to ~ 5 mm in width.

Samples were collected after mapping the profiles across and along the channel. Oriented samples were collected following the standard procedure for AMS sampling (Tarling and Hrouda 1993). This gave a better scope of sampling including the central inner part, the profiles and levees exposure from the top part of the channel. We obtained a total of 280 oriented specimens from 53 sites covering different parts of the lava channel outcrop.

2.1 *Laboratory methods*

The oriented block samples were cored in laboratory to obtain cylindrical specimens of 2.5 cm in

Figure 2. Field exposures of the lava channel depicting the head part in (**A**), the central eroded axial part (**B**), the levee side (**C**) and the end/toe part of the channel (**D**).

diameter and 2.2 cm in height. All the specimens were primarily demagnetised at 100 mT alternating field produced using AGICO (Czech Rep.) LDA 3A alternating field demagnetiser. These specimens were further analyzed for AMS using AGICO KLY-4S Spinner Kappabridge (sensitivity of 2×10^{-8} SI over applied field of 300 A/m at 920 Hz) at the Indian Institute of Geomagnetism, New Panvel (India).

The routine mineral magnetic analysis was conducted at the Paleomagnetic Laboratory of the Department of Geology, Savitribai Phule Pune University (SPPU) to investigate the composition, concentration and domain size variations of the magnetic minerals. The mass-specific susceptibility (X_{lf}) was measured using Bartington MS2B magnetic susceptibility meter at low (0.465 kHz) and high (4.65 kHz) frequencies and its mass normalised values are expressed in 10^{-8} m^3/kg. The anhysteretic remanent magnetisation (ARM) was imparted using AGICO alternating field demagnetiser with 100 mT peak alternating field and 0.1 mT steady bias field; and the remanence was measured using Minispin fluxgate spinner magnetometer (Molspin, UK). The isothermal remanent magnetisation (IRM) was imparted using ASC IM 10–30 impulse magnetiser and the remanence measured using the Minispin spinner magnetometer. The forward fields of IRM were induced

stepwise at 25, 50, 100, 200, 300, 500, 700, 800, 1000, 1500 and 2000 mT. The samples were then demagnetised by a series of back fields of −10, −20, −30, −35, −40, −45, −50 and −100 mT.

AMS and various parameters were derived using standard methods given in Tarling and Hrouda (1993), Cañón-Tapia and Herrero-Bervera (2009), Schöbel and DeWall (2014), Jelinek (1981) and laboratory manuals of AGICO. Principal susceptibility tensors are computed using the least-squares method and accuracy of the anisotropy is evaluated according to the methods described by Hext (1963) and Jelínek (1978, 1981). The data were plotted on the lower hemisphere stereonet projections. For interpretations, the samples were grouped into: (i) levee breccia, (ii) terminal and distal parts of channel flow, (iii) mid-channel and (iv) channel floor/country rocks apart from the entire set of samples as a whole.

3. Results of magnetic mineralogy

Parameters obtained from the rock magnetic analysis were mass normalised and described using routine statistical methods after classification of data into various sampling domains (see tables 1 and 2 in supplementary data file, and figure 1) besides the overall data.

The combined mean mass-specific susceptibility (X_{lf}) for the overall data is 45×10^{-8} m^3/kg with a variation between 171 and 1 $(\times 10^{-8}$ m^3/kg) around median of 17.82 $(\times 10^{-8}$ m^3/kg). The overall X_{lf} thus shows high variability in ferrimagnetic mineral dominance. The distal samples (D series) and samples from channel sides/levees (LB series) show mean X_{lf} of 50 $(\times 10^{-8}$ m^3/kg) within a range from 155 to 2.6 $(\times 10^{-8}$ m^3/kg) with a median of 8.37 depicting large variability similar to the overall data. The country rock basalt (OF series) show significantly high mean X_{lf} of 147, indicating higher ferrimagnetic concentration in the floor relative to the channel.

The IRM spectra of forward and backfields demonstrate the systematic changes in mineralogy from totally ferrimagnetic near the head, to mixed ferri and antiferromagnetic followed by antiferromagnetic dominant mineralogy at the mouth (figure 3). This is also very well supported by the thermomagnetic $(k-T)$ curves (figure 3). The samples from the sites near the head of the lava channel (NG series) show anomalously low mean coercivities $(B_{(0)CR})$ of 9.5 mT varying in the range from 3 to 14 mT and median of 12 mT. The samples from the profile named 'S' (S-series) across the head of the lava channel shows mean X_{lf} of 77 $(\times 10^{-8}$ m^3/kg) within a range of $15-150$ with a median value of 82 $(\times 10^{-8}$ m^3/kg) and is relatively higher than any other profile. Further, the individual sites from the middle part of the lava channel (namely C1, C4, C9, L1, L5, L3 and Q1) show significant drop in X_{lf} with a mean value of 36 and median of 24, ranging from the values as low as 3 to a maximum of 112. These sites therefore show higher coercivities than their preceding sites depicting a change in mineralogy from ferrimagnetic dominant to antiferromagnetic. This implies that the low X_{lf} is controlled by ferrimagnetic to paramagnetic concentration and higher antiferromagnetic content. The magnetic properties of Deccan basalts are characteristic of the titanomagnetite occurrences. The antiferromagnetic (haematite-like mineralogy) signatures from the fresh, unweathered basalts, therefore, pertain to oxidative conditions. As there is no lateritisation observed, the chances of secondary haematite are ruled out. The succeeding sample sites (BG series) show still lower X_{lf} and higher coercivity, further indicating progressive increase in antiferromagnetic concentration within the lava channel. This trend continues with the farthest end (KD series sites).

The samples from SN series indicate some improvement in X_{lf} depicting the mean value of 19 but also record the lowest minimum X_{lf} (~ 1) within the entire sampling for the present study. Thus, we propose high-temperature oxidation as the lava progressed resulting in the formation of haematite. Therefore, the lowering of X_{lf} in the present case can be linked to significant increase in oxidative mixing of the lava. The country rock exposed in similar manner routinely shows higher ferrimagnetic concentration. Figure 3 plots the gradients against distance in the studied rock magnetic parameters discussed further.

The frequency-dependent susceptibility $(X_{fd}\%)$ depicts concentration of grains at domain size boundary of SD-SP, and the X_{ARM} indicates concentration of SD grains under laboratory-induced saturation conditions (Liu *et al.* 2012). The overall sample mean $X_{fd}\%$ is 5% with large variation, and a low median value of 2.7%. This indicates low-to-negligible SP content with considerable amount of SD grains except for the sites D2 and LB which show high X_{fd} of 7.2%. The 100 mT demagnetisation before AMS measurement allowed us to reduce the influence of inverse fabrics from SD grains. The OF series show low value of 3.2% and the S series show the lowest values. The samples of C, Q, L, NG and BG series show similar values with no gradient. The X_{ARM} shows mean value of 13.5 $(\times 10^{-5}$ m^3/kg) with a median of 7.44 varying in the range from 102 to 0.3 $(\times 10^{-5}$ m^3/kg) for the entire data. The D2 and LB samples show moderate–to-low X_{ARM} with mean value of 11.15 $(\times 10^{-5}$ m^3/kg) varying between 43 and 2. The OF series show higher mean X_{ARM} of 46 within a range from 56 to 40 $(\times 10^{-5}$ m^3/kg). The S series show little higher values of 22 with a maximum of 102 $(\times 10^{-5}$ m^3/kg). The C, Q and L show lower values which continue with the NG series, BG and KD showing still lower values.

The overall mean coercivity of remanence $B_{(0)CR}$ shows a value of 111 mT varying in the range from 22 to 440 mT. This clearly indicates a large variation in the magnetic mineralogy from soft ferrimagnetic to hard antiferromagnetic composition. The D2 and LB series (combined) show a mean $B_{(0)CR}$ of 130 mT (median of 137) varying from 40 to 196 mT and depict the presence of haematites. The OF series show low $B_{(0)CR}$ mean of 23.75 mT within a range of $22-27$ mT as these samples are from the channel floor (country rock) indicating typical ferrimagnetic dominant mineralogy of the Deccan traps. This series is further dominated by
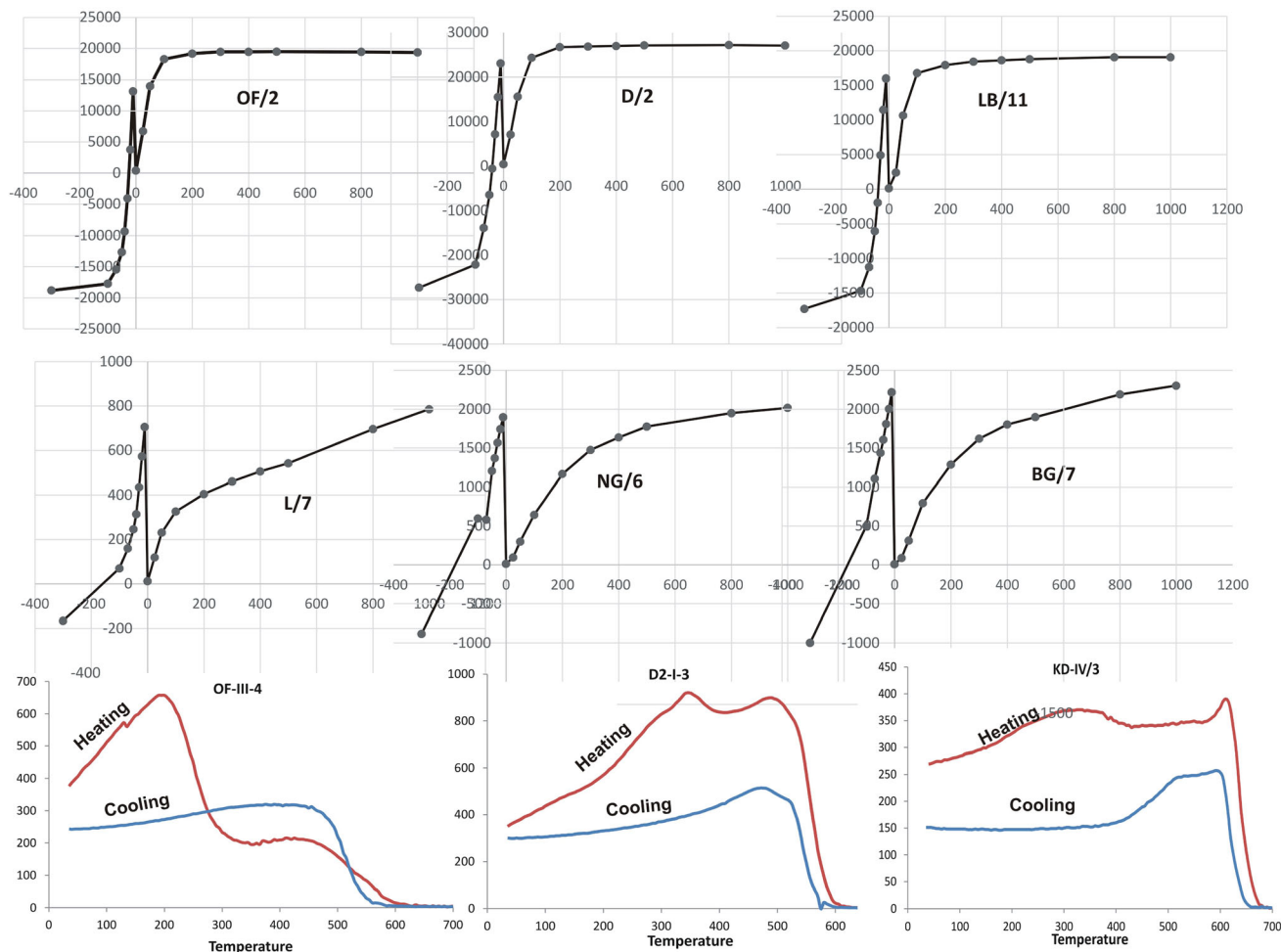
Figure 3. Representative graphs of IRM spectra and the thermomagnetic measurements for the samples from studied lava channel arranged by head towards mouth mainly depicting the major change in mineralogy from ferrimagnetic to antiferromagnetic composition. The units for X-axis in IRM spectra are in mT and the Y-axis represents the induction in AM^2/kg. The thermomagnetic temperature scale represents degree centigrade and the Y axis is volume susceptibility in 10^{-6} CGS units.

larger domain size (MD) as against the channel showing a mix of hard (SD) and MD ferrimagnets depict relatively rapid cooling in the channel.

The S-series show a mean $B_{(0)CR}$ of 42 mT (varying between 32 and 77 mT) and suggest a mixture of hard ferrimagnetic and antiferromagnetic minerals. The C, Q and L (combined mean) show gradual higher values of $B_{(0)CR}$ (mean: 81 mT, median: 52 mT, maximum: 202 mT) depicting an increased antiferromagnetic content. The NG series further shows a gradual increase in $B_{(0)CR}$ (mean: 86, median: 39 and maximum: 182). This is followed by the BG series showing further enhancement of coercivity to 253 mT (mean) with a range from 164 to 340 mT indicating dominant antiferromagnetic mineralogy. This trend continues with the KD series showing a mean $B_{(0)CR}$ of 252 mT in the range from 178 to 301 mT. The SN series show a decrease in coercivity to 148 mT (mean) but record the highest maximum coercivity of 440 mT. The BB series shows a mean of 139 mT varying in the range from 70 to 197 mT. This establishes a progressive increase in coercivity from the head towards the channel mouth (figure 4) as a result of increasing antiferromagnetic mineralogy (s.s. haematite) substantiating the inferences above.

The S-ratio is another parameter to decipher the compositional as well as domain size variation within the ferri- or antiferromagnetic mineralogy. The mean S-ratio of −0.25 with a minimum and maximum of −1 to 0.85 for all the samples combined indicates a mixed ferri to antiferromagnetic mineralogy with a variety of domain sizes. The D2 and LB series combined shows still lower negative mean of −0.15 with a range from −0.82 to 0.47;
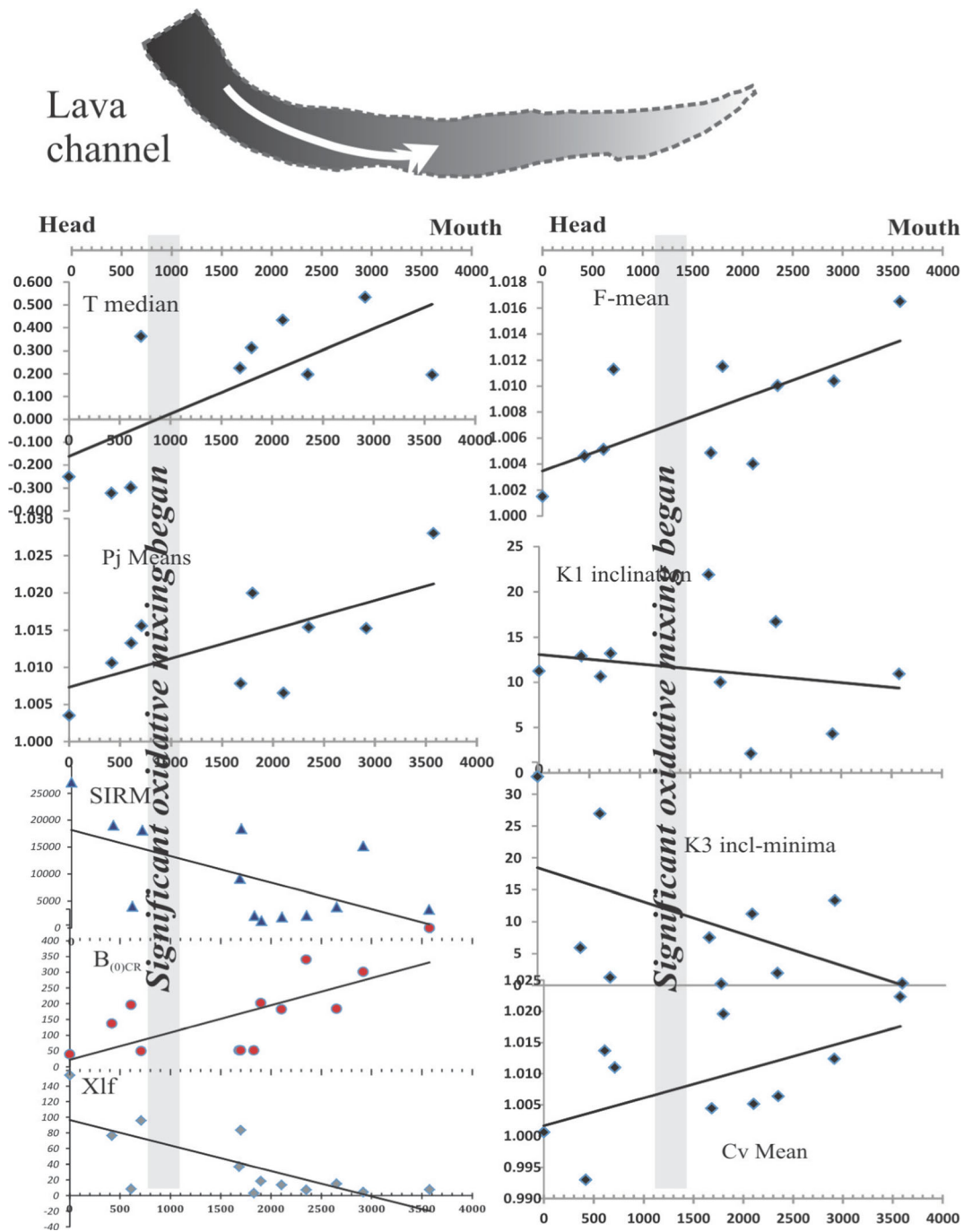
Figure 4. Distance *vs.* amplitude plots of fundamental rock magnetic and AMS parameters for the studied lava channel depicting large-scale gradient.

indicating a range of domain sizes from MD to SD ferrimagnet and the antiferromagnetic concentration.

The OF series show a mean S-ratio of −0.92 within the range of −0.93 to −0.9 depicting uni-modal MD ferrimagnetic mineralogy for the floor basalt. The samples from S series have a mean S-ratio of −0.7 varying between −1 and −0.22 and indicate a range of ferrimagnetic domain size from PSD, SD to MD. The combined values of the samples C, Q and L show a mean S-ratio of 0.33 varying between −0.8 and 0.39 indicate mixed composition with dominant antiferromagnetic contribution from haematite. The BG series displays a positive mean S-ratio of 0.53 varying between 0.22 and 0.75 to indicate entirely antiferromagnetic mineralogy. The KD series indicate positive S-ratio with a mean of 0.27 within a range of 0−0.5 indicating antiferromagnetic mineralogy.

The samples of SN series have a low negative S-ratio from −0.7 to 0.81 depicting a mixed ferri- and antiferromagnetic mineralogy. Whereas, BB series show a positive mean S-ratio of 0.11 with a variation from −0.42 to 0.47 indicating predominant antiferromagnetic mineralogy. As a result, the S-ratio variation along the channel demonstrates gradient from head towards mouth (figure 4) in agreement with other parameters.

The mean SIRM for the combined data is 9116 ($\times 10^{-5}$ AM^2/kg) with a large variation from 28,856 to 785 ($\times 10^{-5}$ AM^2/kg). The D2 and LB series samples (grouped) show high mean SIRM of 10,872 ($\times 10^{-5}$ AM^2/kg) with variation between 27,058 and 1658 ($\times 10^{-5}$ AM^2/kg). The OF series further show very high ferrimagnetic concentration indicated by the mean value of 17,424 ($\times 10^{-5}$ AM^2/kg) with low variability between 15,472 and 19,338 ($\times 10^{-5}$ AM^2/kg). The S-series showed a moderate value with a mean of 13,308 ($\times 10^{-5}$ AM^2/kg) within a range from 5986 to 27,016. The samples C, Q and L combined depict a mean value of 8305 within a range from 28,856 to 785 indicating progressive decrease in ferrimagnetic concentration.

The soft-IRM depicting ferrimagnetic concentration shows a mean value of 1987 for all the samples combined. It shows a mean value of 2002 for the D2 and LB combined, while the OF series shows a higher mean value of 7203. The S-series show a lower mean value of 3007 which again decreases to 1430 for C, Q and L combined series. The NG series record a notable decrease in soft-IRM to a mean value of 273, which is further reduced to 104 in the succeeding samples of BG series. The KD series show an improvement in soft IRM by depicting the mean value of 2346. The SN series however show further decrease in mean value to 8572 that continued with similar decrease in BB series showing a mean value of 806. Thus there is clear decreasing gradient for the soft ferrimagnetic mineralogy from head towards mouth.

The hard IRM shows a mean value of 623 for all the samples combined. The D2 and LB series (combined) show a value of 521 for hard IRM, whereas the OF series showed a still lower value of 239. The S-series further depict the low value of hard IRM of 315. The NG series also depict higher value of 404 with further increase to 689 in BG series. The KD series showed significant increase in hard-IRM by showing a value of 3028 and recording the highest value of 7624. The SN series record

a low value of 525, while the BB series show improvement to 846.

The SIRM/X_{lf} showed a mean value of 505 (10^3 A/m) for all the samples combined and lower value of 381 for the D2 and LB combined. The OF series showed low SIRM/X_{lf} of 119 due to its ferrimagnetic mineralogy. The S-series shows a little improvement to 295 and BG series records significant increase in the SIRM/X_{lf} ratios to 565. Furthermore, the KD series have shown a mean value of 3295. The SN series show lower values of 658 (mean), whereas BB series show further lower values of 332 clearly depicting the gradient.

The rate of IRM acquisition (RPM factors) depicts maximum acquisition at 100–500 mT followed by 200–100 mT; and thereafter gradual decreasing order for D2 and LB combined, OF series, S-series, C, Q, L combined. However, the NG series show two clear trends marked by an increase at RPM 800–500. Similar trend is shown by the BG series, whereas the KD series showed one more additional increase at RPM 1000–800. The SN series showed two trends as above.

Overall the rock magnetic parameters have shown notable gradient of ferrimagnetic/antiferromagnetic mineralogy and its concentration.

4. AMS variation

The AMS is an advanced approach for the study of petrofabrics and estimation of strain parameters, deformation patterns and flow-related fabrics. The flow-related fabrics are often heterogeneous; and need to be studied at various scales (orders) depending upon the case study. For the present channel body therefore we adopted first-order, second-order and third-order interpretation of the fabrics. The detailed data in tabular form is given in table 3 of the supplementary data file.

4.1 *The first-order fabric development*

The first-order approach was made by observing and averaging the data along the channel and focusing on D/I values of principle susceptibility axes. Figure 5 represents the contours for D/I vectors of K1 and K3 in the lower hemisphere. The K1 shows distribution around northern and southern poles and is parallel−subparallel to the channel axis. The K3 is clustered around the centre
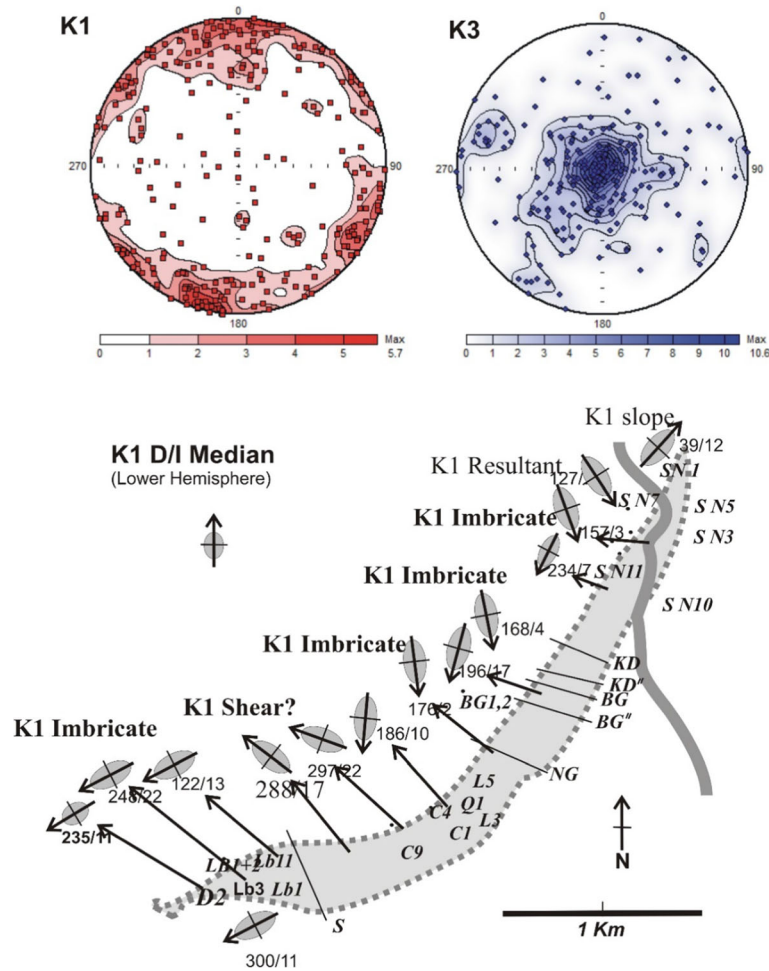
Figure 5. Lower hemispheric presentation of the contour plots for the principle susceptibility axes K1 and K3. The lower diagram shows localised ellipsoids for the channel depicting various possible effects of the flow dynamics discussed in the text.

of the stereonet plot indicating steep inclinations, and the contours further show tilt bias in the southern hemisphere. The K1 is generally down tilted in the southern hemisphere. Further, the localised averages are plotted all along the channel length to depict the regional distribution of the principal axis (see figure 5). The higher part of the channel clearly shows headward dipping K1 indicating imbrication in the flow direction. This follows another distribution of K1 which is perpendicular to channel flow suggesting viscosity shear which might result into the orientation of K1 in easy direction, i.e., perpendicular to channel flow. Further downwards the predominance of K1-imbricated fabric is continued as the channel progressed. At the end of the channel, there is clear north dipping K1 suggesting a gravity slope-type fabrics. Thus, the first-order observation indicates dominantly imbricate nature of the fabric in the flow direction. This suggests flow-related viscous

push driving the shear and gravity in the flow direction.

4.2 Second-order fabric development

The second-order distribution is observed at the profile level and by grouping the samples according to depositional environment such as levees, central part of the channel, channel head, etc. In this order, the fabrics are dominated by oblate nature with steep inclinations of K3 and shallow K1 and K2 axes. The scatter in the direction of K1 axis, progressively amongst individual sites is anticipated due to curvilinear geometry of the Khedrai channel body. The grouped and site-wise distribution of the fabrics is given below.

The topmost site D2 falls near the head and shows predominant imbrication of K1 axis (dipping SW) and K3 dipping SE, largely agreeing with the flow direction and suggest a resultant fabric. The

OF series is from the basalt floor and displays random fabric. The S series cross profile shows high inclination for K3 axis (depicting oblate nature), while K1 and K2 are dispersed. The mean of K1 axes shows NW dip, depicting its linearity with the flow direction. The C series also show K1 linearly oriented in the flow direction. The Q series show an imbrication fabric with shallow dip of K1 axis towards the head. Furthermore, the L series show K1 linearly oriented to the flow direction. The NG series show K1 axis dipping towards the head as an imbrication fabric. The BG series show head dipping imbrication of K1 axis, whereas KD shows a large scatter except K3 showing high inclination and K1 and K2 axes are distributed with shallow inclinations. The SN series also shows the distribution of K1 and K2 axes with high inclination for K3 axis. The above distribution of the fabrics broadly indicated persistently steep and well-clustered K3 axis and shallow inclinations with scatter for K1 and K2 depict the oblate fabrics. The K1 axis appears to change its behaviour from 'imbrication type' to 'lineation type' showing the south-dipping and north dipping attitudes in the flow direction, although consistently shows the shallow inclinations.

To critically examine the scatter of fabrics, we further plotted the sites on the studied profiles (figure 6a–e). The left part of profile S was sampled, as the central part and the right side did not permit sampling due to vegetation and thick colluvium cover (figure 6a). The specimens from samples S1 and S2 were grouped, which is the inner part of the left side of the channel (figure 6a). This part shows imbrication by south-dipping K1 axis. The samples S3−S5 are also marked by south-dipping K1, but with orientation perpendicular to the channel (figure 6a). This heterogeneity can be explained as the site is very near to the head resulting in turbulence. The central part of the channel represented by BG3 in the BG' profile shows inclination of K1 dipping south depicting imbricate fabric (figure 6c). The right-side sites (BG5 and BG7) in the BG profile show K3 falling at the centre with mixed and shallow K1 and K2, depicting oblate fabrics (figure 6d). The samples from KD profile falling in the central part of the channel show highly scattered K1 and fairly well-clustered K2 and K3 axes falling at the centre.

The above results depict moderate-to-fair clustering of the principle susceptibility axes within the sample as well as amongst the sites, although the K3 axis remains well clustered due to high inclinations (upright) in agreement with the oblate fabrics. Such variability can be attributed to crystal settling as the chief mechanism of the fabric development. This proposes that majority of the fabrics were developed during penultimate stage of cooling of the lava and during its partial residency.

4.3 Third-order fabrics development

We further examined petrographic (mineralogical and textural interrelations) of the opaque−non-opaque constituents within the samples to infer its relation with AMS (figure 7). We find that plagioclase represents the most anisotropic (lath-shaped) mineral but with a variety of orientations. Plagioclase also represents paramagnetic minerals and does not contribute to AMS when it is strongly controlled by ferrimagnetism. In few samples, the opaque minerals (spinel group) representing titanomagnetites are aligned with some of the plagioclase laths or occur tightly occupied in the interstices of the paramagnetic minerals producing a resultant anisotropy.

The S/N Q1a (figure 7) showed hard ferrimagnetic composition with oblate fabrics having K1 aligned in the direction of the channel flow. The sample Q1d shows similar rock magnetic properties to that of Q1a, but with K1 sub-parallel to the flow direction. The plagioclase laths compete with the opaque minerals which fill the spaces in majority of the samples. However, some euhedral opaque grains are also seen without any sympathetic orientation with plagioclase laths in some samples. The sample S/N 3a shows very low susceptibility but higher coercivity indicating the existence of haematites. The sample D2a is from the head and shows the highest susceptibility with ferrimagnetic coercivities and representing prolate fabrics.

The varied association of opaque grains with non-opaque matrix suggests a variety of mechanisms for fabric development, yielding the heterogeneity and scatter amongst fabrics in the channel body. The fabrics sympathetic to the plagioclase laths are influenced by the style of settling. The samples with euhedral crystals behave indifferent to the fabrics created by laths and this is common near the head part. Haematite has influenced the susceptibility to be weakened but the fabric remains unaffected from haematite and appears to be largely controlled by the ferromagnetic constituents. The occurrence of oblate fabrics with K1 and K2 axes falling near the great circle (shallow inclinations) suggests crystal settling as the chief mechanism of control of AMS. This fabric
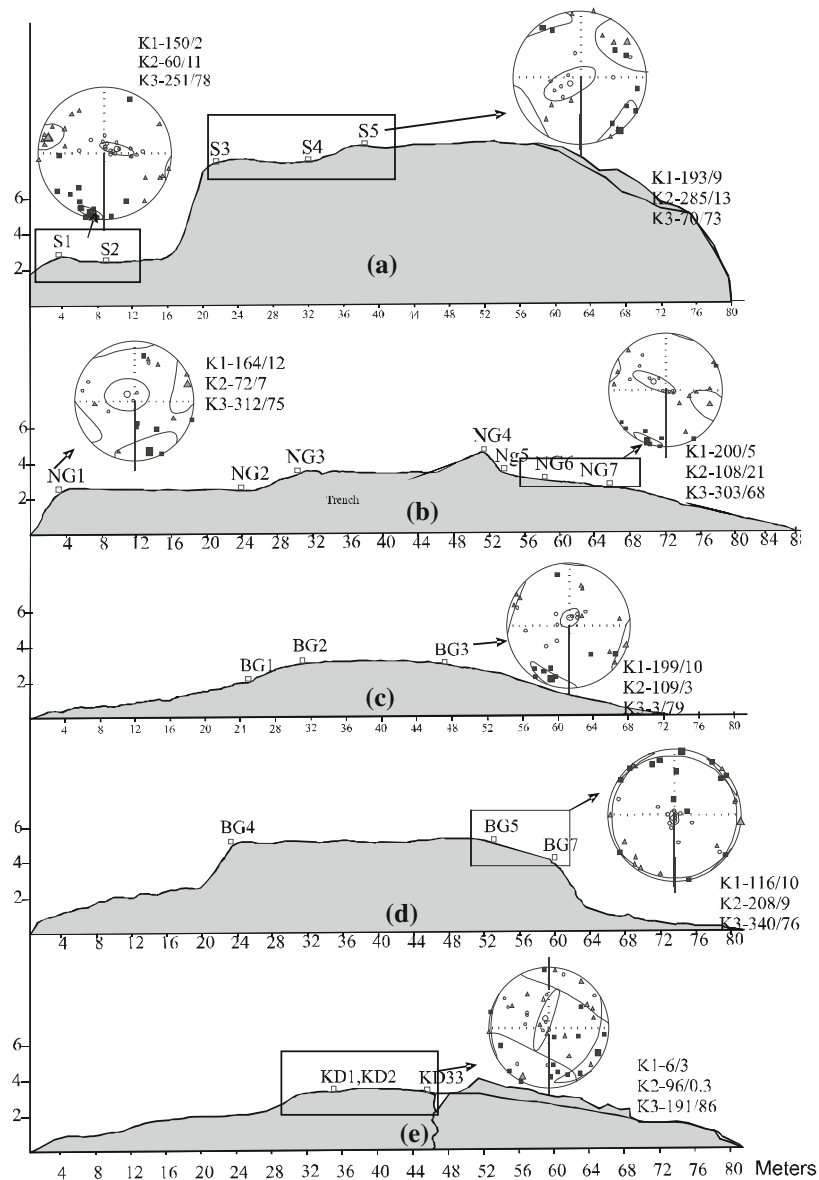
Figure 6. Site-wise location of the fabrics in representative profiles (marked in figure 1). Details are discussed in the text.

development occurred during the lava residence stage before cooling. Some fabrics show orientation of K1 axis in the direction of flow indicates the resultant of crystal settling and flow vector. Although the mineralogy has unequivocally changed from dominant ferrimagnetic to antiferromagnetic during lava progression, the latter did not affect the fabrics that are generally governed by ferromagnetic constituents.

5. An insight into the fabric development in lava channel

Lava flow in the form of a channel is a dynamic system where the viscosity and temperature gradients are changing continuously. The lava flow contains rapidly quenching silicate melts and follow the crystallisation temperatures of various melt components possibly causing rapid fractionation towards surface temperatures. The minerals of spinel group in basaltic groundmass are quenched first and thus are ready for the formation of initial fabrics. These minerals being magnetically representative, record the mechanism of cooling and fabric development till the final stages of cooling and solidification. Further, in the lava flows, it is anticipated to have viscosity shear as the chief mechanism to alter the initial fabric (if any) and reorient the mineral grains. We however find gravity settling as dominating phenomenon to impart the fabric which can occur during the brief residency of the lava but competing with any formerly
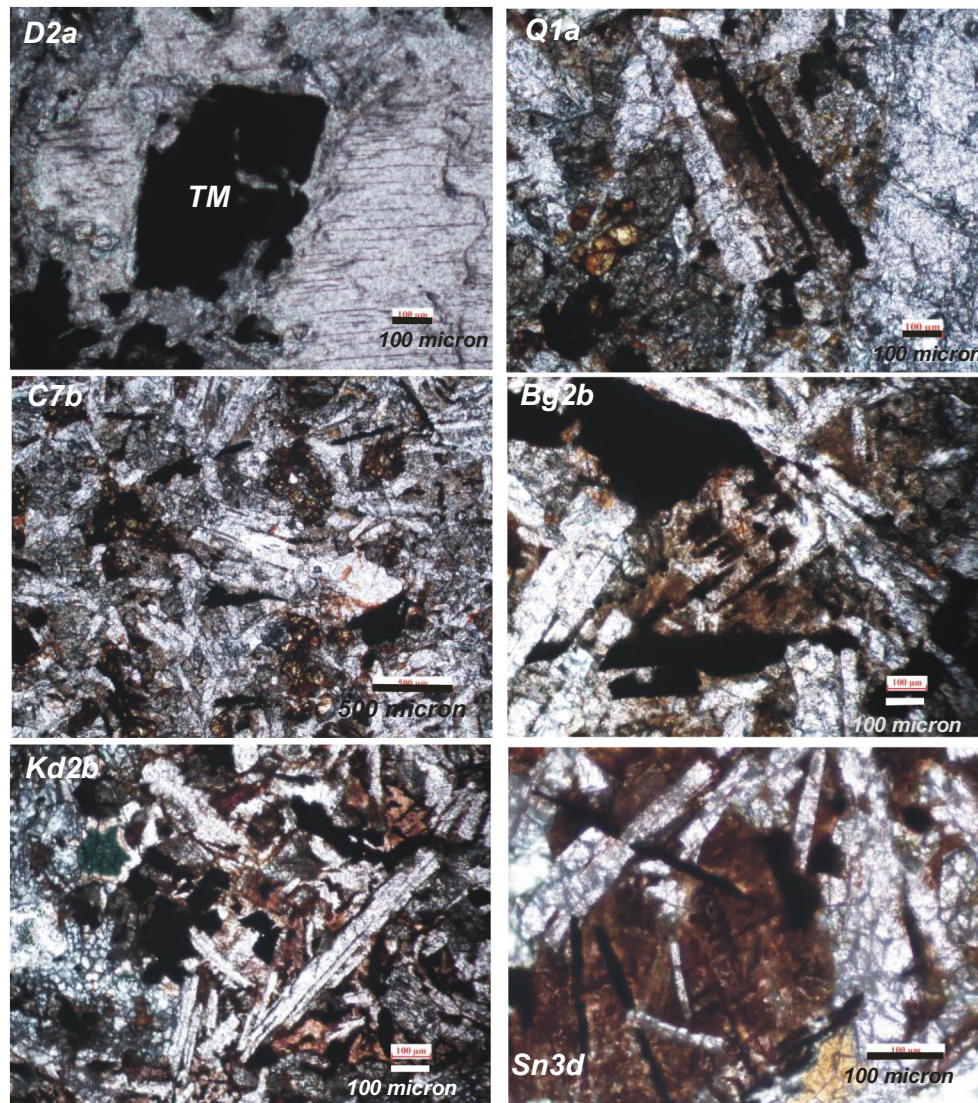
Figure 7. Photomicrographs showing possible mechanism of the AMS fabric built-up. Details are discussed in the text.

developed fabrics (figure 8). This stage is influenced by the flow in relatively higher viscosity conditions as the silica enrichment vis-à-vis cooling trend of the lava flow are equilibrated. In this stage and up to the complete solidification, the earlier stage of gravity settling appears to have been further modified to represent the AMS fabrics as a combination of mineral lineation, imbrication by the cluster of minerals and viscosity shear. In our results, we find the imbrication as the most dominating fabric which can develop penultimate to crystal readjustments. The imbrication fabric produces most significant information related to the flow directions. On the contrary, the dominant oblate fabrics with high K3 inclinations depict crystal settling. The crystal settling can occur during brief residence of the lava flow penultimate

to cooling. Many sites especially in the central part of the channel have shown a fabric marked by K1 imbrications and lineation. The fabric heterogeneity in the lava flows is because of the spatial distribution of different higher-order processes as well as overprinting of two or more fabrics to produce a resultant. Based on all these observations, the magnetic fabric data from the studied lava flow have been classified into the following three types displayed by the principle susceptibility axis K1.

5.1 Type I: Lineation type

This fabric shows a moderate-to-weak lineation of the K1 axis, parallel to the lava flow direction and the K3 remaining upright under low degree of foliation. K1 shows weak-to-moderate imbrication
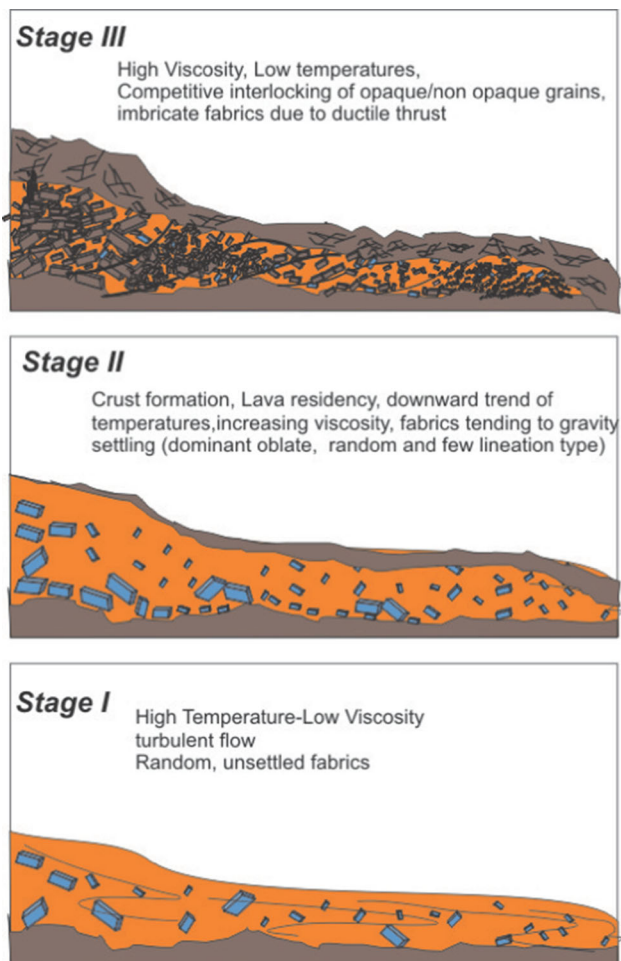
Figure 8. A hypothetical cartoon model based on the inferences of AMS under various conditions of the lava flow dynamics.

in the flow direction. This type of fabric is generally observed in the central axial part of the channel. This suggests that some of the grains during settling are oriented by the flow.

5.2 *Type II: Random/crystal settling type*

This fabric is dominantly observed in the levee part and the marginal part of the lava channel. This fabric typically shows oblate nature with randomness arising from a combination of turbulence and slope effects at the channel margin.

5.3 *Type III: Crystal-matrix adjustment type*

This fabric observed from the petrographic thin sections shows the adjustment of the opaque and non-opaque grains and matrix indicating crystal adjustment during the final stages of cooling resulting mostly into random fabrics.

5.4 *Type IV: Imbrication fabrics*

These fabrics are developed at the penultimate stage of cooling from any of the above types during non-buoyant ductile thrust. This fabric is developed by the force vector directed from the head towards the mouth, which is the resultant of gravity and material push.

Thus, the overall persistent shallow inclinations for K1 and K2, and upright K3 indicate the absence of any major imprints of the viscosity shear that may otherwise develop strong imbrications or a strong flow perpendicular-type I fabrics (K1 perpendicular to the flow direction). This depicted that the fabrics are developed at various stages during the lava flow, lava residency and before cooling. There is significant change in viscosity during all these stages and the fabrics due to viscous shear tend to alter by later processes.

The petrographic observations attest interlocking of plagioclase laths with opaque minerals to influence the ferrimagnetic fabrics largely leading to resultant or randomisation of fabrics (types II and III). The study infers that the magnetic fabrics in the given lava channel is proxy to petrofabrics formed during penultimate stages of cooling. Although the given lava channel cannot be generalised for the average lava flows in the Deccan stratigraphy, the present work explains the spatio-temporal development of a large variety of fabrics in the Deccan traps that can be characteristic of the given lava flow.

We suggest that detailed AMS studies on various lava flows can address the data-based relative estimates on fluid dynamical forces, the effects of gravity and slope gradients, the effects of dynamic viscosity changes and shear in the background of dynamic changes in thermal gradients. The role of quenching of silicate melt on mineral-space readjustments to influence the fabric needs to be examined. More studies can help in the identification of strained and unstrained basalts further to estimate the strain-related parameters in these rocks. Nevertheless, reporting the AMS data with these various considerations can help to characterise the extensive lava flow formations in the DVP as a rapid method.

6. Conclusion

The combined rock magnetic and AMS studies conducted over a lava channel in the DVP produce an insight into systematic changes in magnetic

mineralogy and the variability amongst the AMS fabrics. The rock magnetism indicated distinct mineralogical gradient from ferrimagnetic at the head to antiferromagnetic towards the mouth of the channel indicating oxidative mixing as the lava progressed. The AMS showed oblate, imbricate and resultant fabrics due to a combination of several spatio-temporally dominating processes leading to lineation type, random/crystal settling type and crystal adjustment-type fabrics. This study attempted to visualise the various overprinting phenomena of fabric development; during the initial channel flow, lava residency and lava cooling and proximal, distal, channel central and levee locations at dynamic temperature and viscosity conditions. The petrographic observations depict crystal adjustments to create resultant or randomisation of initial fabrics giving rise to large variability at the sample level.

Overall, we infer that the competitive conditions amongst fluid dynamical forces, gravitational force, temperature gradients, dynamic viscosity and decreasing accommodation spaces penultimate to cooling are the deciding factors to impart the final petrofabrics in lava flows.

Acknowledgements

Author statement

S J Sangode: Conceptualisation, funding acquisition, planning, administration, interpretation and writing. Sayelli Tembhurne: Analysis, interpretation and writing. Rasika Mahajan: Fieldwork, analysis, interpretations. K Deenadayalan: Laboratory analysis, interpretations, writing. D C Meshram: Fieldwork, analysis, writing. A N Dongre: Interpretation, writing. Amarjeet R Bhagat: Analysis, interpretation, writing. K V V Satyanarayana: Interpretation, writing.

References

Bascou J, Camps P and Dautria J 2005 Magnetic versus crystallographic fabrics in a basaltic lava flow; *J. Volcanol. Geotherm. Res.* **145(1)** 119–135.

Beane J E and Hooper P R 1986 Picrite basalts in the Deccan traps: Primary magmas or cumulates?; *Int. Vol. Canol. Congr. (IAVCEI), Auckland (abstract volume),* 346p.

Bondre N R, Duraiswami R A and Dole G 2004 Morphology and emplacement of flows from the Deccan Volcanic Province, India; *Bull. Volcanol.* **66** 29–45.

Callot J P, Geoffroy L, Aubourg C, Pozzi J P and Mege D 2001 Magma flow directions of shallow dykes from the East Greenland volcanic margin inferred from magnetic fabric studies; *Tectonophys.* **335(3)** 313–329.

Cañón-Tapia E 1994 AMS parameters: Guidelines for their rational selection; *Pure Appl. Geophys.* **142** 365–382.

Cañón-Tapia E 1996 Single-grain versus distribution anisotropy: A simple three-dimensional model; *Phys. Earth Planet. Inter.* **94(1)** 149–158.

Cañón-Tapia E and Coe R 2002 Rock magnetic evidence of inflation of a flood basalt lava flow; *Bull. Volcanol.* **64** 289–302.

Cañón-Tapia E and Herrero-Bervera E 2009 Sampling strategies and the anisotropy of magnetic susceptibility of dykes; *Tectonophys.* **466(1)** 3–17.

Cañón-Tapia E and Pinkerton H 2000 The anisotropy of magnetic susceptibility of lava flows: An experimental approach; *J. Volcanol. Geotherm. Res.* **98(1)** 219–233.

Chenet A L, Courtillot V, Fluteau F, Gérard M, Quidelleur X, Khadri S F R, Subbarao K V and Thordarson T 2009 Determination of rapid Deccan eruptions across the Cretaceous–Tertiary boundary using paleomagnetic secular variation: 2. Constraints from analysis of eight new sections and synthesis for a 3500-m-thick composite section; *J. Geophys. Res.* **114/38**, https://doi.org/10.1029/2008JB005644.

Chenet A L, Fluteau F, Courtillot V, Gerard M and Subbarao K V 2008 Determination of rapid eruption across the Cretaceous–Tertiary boundary using paleomagnetic secular variation: Results from a 1200 m thick section in the Mahabaleshwar escarpment; *J. Geophys. Res.* **113(B4)** B04101.

Cox K G and Hawkesworth C J 1985 Geochemical stratigraphy of the Deccan traps at Mahabaleshwar, Western Ghats, India, with implications for open system magmatic processes; *J. Petrol.* **26(2)** 355–377, https://doi.org/10.1093/petrology/26.2.355.

DeWall H, Schöbel S, Pandit M K, Sharma K K and Just J 2010 A record of ductile syn-intrusional fabrics to post solidification cataclasis: Magnetic fabric analysis of Neoproterozoic Mirpur and Mt. Abu Granitoids, NW India; *J. Geol. Soc. India* **75(1)** 239–253.

Dongre A, Dhote P, Zamarkar P, Sangode S J, Belyanin G, Meshram D C, Patil S K, Karmakar A and Jain L 2021 Short-lived alkaline magmatism related to réunion plume in the Deccan large igneous province: Inferences from

petrology, 40Ar/39Ar geochronology and paleomagnetism of lamprophyre from the Sarnu-Dandali alkaline igneous complex; *Geol. Soc. London, Spec. Publ.* **513**, https://doi.org/10.1144/SP513-2021-34.

Dragoni M, Lanza R and Tallarico A 1997 Magnetic anisotropy produced by magma flow: Theoretical model and experimental data from Ferrar dolerite sills (Antarctica); *Geophys. J. Int.* **128(1)** 230–240.

Duraiswami R A, Gadpallu P, Shaikh T N and Cardin N 2014 Pahoehoe–a' a transitions in the lava flow fields of the western Deccan traps, India − implications for emplacement dynamics, flood basalt architecture and volcanic stratigraphy; *J. Asian Earth Sci.* **84** 146–166.

Ellwood B B 1981 Weathering effects on the magnetic properties of the Milledgeville granite, Georgia; *Earth Planet. Sci. Lett.* **55** 311–316.

Font E, Adatte T, Andrade M, Keller G, Ambabi B, Carvallo C, Ferreira J, Diogo Z and Mirão J 2018 Deccan volcanism induced high-stress environment during the Cretaceous–Paleogene transition at Zumaia, Spain: Evidence from magnetic, mineralogical and biostratigraphic records; *Earth Planet. Sci. Lett.* **484** 53–66.

Geoffroy L, Callot J P, Aubourg C and Moreira M 2002 Magnetic and plagioclase linear fabric discrepancy in dykes: A new way to define the flow vector using magnetic foliation; *Terra Nova* **14(3)** 183–190.

Godbole S M, Rana R S and Natu S R 1996 Lava stratigraphy of Deccan basalts of Western Maharashtra; *Gondwana Geol. Mag. Spec.* **2** 125–135.

Hargraves R B, Johnson D and Chan C Y 1991 Distribution anisotropy: The cause of AMS in igneous rocks?; *Geophys. Res. Lett.* **18(12)** 2193–2196.

Herrero-Bervera E, Walker G P L, Canon-Tapia E and Garcia M O 2001 Magnetic fabric and inferred flow direction of dikes, conesheets and sill swarms, Isle of Skye, Scotaland; *J. Volcanol. Geotherm. Res.* **106(3)** 195–210.

Hext G R 1963 The estimation of second-order tensors, with related tests and designs; *Biometrika* **50(3–4)** 353–373.

Hooper P R 1990 The timing of crustal extension and the eruption of continental flood basalts; *Nature* **349** 246–249.

Jelínek V 1978 Statistical processing of anisotropy of magnetic susceptibility measured on groups of specimens; *Stud. Geophys. Geod.* **22** 50–62.

Jelinek V 1981 Characterization of the magnetic fabric of rocks; *Tectonophys.* **79** 63–67.

Liu Q, Roberts A P, Larrasoaña J C, Banerjee S K, Guyodo Y, Tauxe L and Oldfield F 2012 Environmental magnetism: Principles and applications; *Rev. Geophys.* **50** RG4002, https://doi.org/10.1029/2012RG000393.

Mahoney J J 1988 Deccan traps; In: *Continental flood basalts* (ed.) Macdougall J D, Kluwer Acad, Dordrecht, pp. 151–194.

Majumder S and Mamtani M A 2009 Magnetic fabric in the Malanjkhand granite (Central India) − implications for regional tectonics and Proterozoic suturing of the Indian shield; *Phys. Earth Planet Inter.* **172(3–4)** 310–323, https://doi.org/10.1016/j.pepi.2008.10.007.

Mamtani M A and Greiling R O 2005 Granite emplacement and its relation with regional deformation in the Aravalli Mountain Belt (India) − inferences from magnetic fabric; *J. Struct. Geol.* **27(11)** 2008–2029.

Mishra K S, Sabale A B and Bhutani R 2001 Lava channels and tubes in the western part of the Deccan Volcanic Province; *Geol. Survey India, Spec. Publ.* **64** 503–510.

Nair K K K and Bhusari B 2001 Stratigraphy of Deccan traps: A review; *Geol. Surv. India, Spec. Publ.* **64** 477–492.

Park J K, Tanczyk E I and Desbarats A 1988 Magnetic fabric and its significance in the 1400 Ma Mealy diabase dykes of Labrador, Canda; *J. Geophys. Res.* **93(B11)** 13,689–13,704.

Radhakrishna T, Mohamed A R, Venkateshwarlu M and Soumya G S 2020 Low geomagnetic field strength during End-Cretaceous Deccan volcanism and whole mantle convection; *Sci. Rep.* **10** 10743, https://doi.org/10.1038/s41598-020-67245-6.

Rochette P, Jackson M and Aubourg C 1992 Rock magnetism and the interpretation of anisotropy of magnetic susceptibility; *Rev. Geophys.* **30(3)** 209–226.

Rochette P, Jenatton L, Dupuy C, Boudier F and Reuber I 1991 Diabase dikes emplacement in the Oman ophiolite: A magnetic fabric study with reference to geochemistry; In: *Ophiolite genesis and evolution of the oceanic lithosphere* (eds) Peters T, Nicolas A and Coleman R G, Kluwer Academic Publishers, Dordrecht, pp. 55–82.

Sangode S J, Sharma R, Mahajan R, Basavaiah N, Srivastava P, Gudadhe S G, Meshram D C and Venkateshwarulu M 2017 Anisotropy of magnetic susceptibility and rock magnetic applications in the Deccan volcanic province based on some case studies; *Geol. Soc. India* **89(6)** 631–642.

Schöbel S and DeWall H 2014 AMS − NRM interferences in the Deccan basalts: Towards an improved understanding of magnetic fabrics in flood basalts; *J. Geophys. Res.* **119(4)** 2651–2678.

Sen B, Sabale A B and Sukumaran P V 2012 Lava channel of Khedrai Dam, northeast of Nasik in western Deccan volcanic province: Detailed morphology and evidences of channel reactivation; *Geol. Soc. India* **80(3)** 314–328.

Stephenson A 1994 Distribution anisotropy: Two simple models for magnetic lineation and foliation; *Phys. Earth Planet. Inter.* **82** 49–53.

Subbarao K V (ed.) 1988 Deccan flood basalts; *Geol. Soc. India Memoir* **10** 393p.

Tarling D H and Hrouda F 1993 *The magnetic anisotropy of rocks*; Chapman & Hall, London, 217p.

Tauxe L, Gee J S and Staudigel H 1998 Flow directions in dikes from anisotropy of magnetic susceptibility data: The bootstrap way; *J. Geophys. Res.* **103(B8)** 17,775–17,790.

Vandamme D, Courtillot V, Besse J and Montigny R 1991 Palaeomagnetism and age determinations of the Deccan traps (India); results of a Nagpur–Bombay traverse and review of earlier work; *Rev. Geophys.* **29** 159–190.

Zak J, Verner K and Tycova P 2008 Multiple magmatic fabrics in plutons: An overlooked tool for exploring interactions between magmatic processes and regional deformation?; *Geol. Mag.* **145(4)** 537–551.

Zhang J and Piper J D A 1994 Magnetic fabric and postorogenic uplift and cooling magnetisations in a Precambrian granulite terrain: The Datong-Huai'an region of the North China Shield; *Tectonphys.* **234(3)** 227–246.

Corresponding editor: N V CHALAPATHI RAO